

# A novel approach to radiographic detection of growth development period with hand-wrist radiographs: A preliminary study with ImageJ imaging software

Samed Şatir<sup>1</sup> | Muhammed Hilmi Büyükçavuş<sup>2</sup>  | Ömer Faruk Sari<sup>2</sup> | Tansu Çimen<sup>1</sup>

<sup>1</sup>Department of Oral and Maxillofacial Radiology, Alanya Alaaddin Keykubat University, Antalya, Turkey

<sup>2</sup>Department of Orthodontics, Suleyman Demirel University, Isparta, Turkey

## Correspondence

Muhammed Hilmi Buyukcavus,  
Department of Orthodontics, Faculty of Dentistry, Suleyman Demirel University, Isparta 32040, Turkey.  
Email: [mhbuyukcvs@gmail.com](mailto:mhbuyukcvs@gmail.com)

## Funding information

This research did not receive any specific grant from funding agencies in the public, commercial, or not-for-profit sectors.

## Abstract

**Objective:** The purpose of this study is to determine whether or not the ImageJ program can be used to automatically determine the growth period of the hand and wrist which have different growth-development periods according to the density values in the phalanges in radiographs.

**Setting and sample population:** Our study included hands-wrist radiographs of 270 individuals aged 8–17 years.

**Material and Methods:** The study's participants were classified into 7 groups according to their skeletal maturation stage (PP2=, MP3=, MP3cap, DP3u, PP3u, MP3u, and Ru) which included pre-peak, peak, and post-peak periods. The total density values (TDV) and pure density values (PDV) in the distal, medial, and proximal phalanges were calculated using each radiograph in the ImageJ program. Analysis of variance (ANOVA) was used to evaluate the density values and chronological age, and pairwise comparisons were made using the post-hoc LSD test.

**Results:** The total density value was graphically zigzagged in the mesial, distal, and proximal phalanges. However, the pure density value increased continuously until the post-peak period and decreased after the DP3u period until the Ru period. While no significant difference in total density values was observed between the growth periods for all three phalanges, a significant difference in pure density values was observed.

**Conclusion:** It has been demonstrated in the ImageJ program that the peak growth period can be distinguished using the pure density values obtained from all phalanges of the third finger and that this method can be used as an alternative to the growth period detection through artificial intelligence.

## KEYWORDS

artificial intelligence, growth and development, hand-wrist radiographs, ImageJ, orthodontics

## 1 | INTRODUCTION

Determining the age of children is necessary in order to conduct clinical evaluations in fields such as paediatrics, orthodontics, forensic sciences, and anthropology. On the other hand, genetic, hormonal, racial, environmental, and nutritional differences can result in variability in young people's chronological age and physiological maturation. In addition, if a reliable method for determining chronological age determination based on physiological parameters is available, changes in the growth rate of adolescent individuals can be closely monitored.<sup>1</sup>

Bone age, which determines skeletal maturation from hand-wrist radiographs, is critical for revealing changes in children's growth and development.<sup>2</sup> Bone age is determined using two distinct methods: Greulich and Pyle (GP) and Tanner-Whitehouse (TW3). Among these, the GP atlas is generally accepted as the more practical and straightforward method and this is widely used in clinical practice.<sup>3</sup> Apart from this, various researchers established numerous methods for determining growth periods and bone age. However, assessing bone age through observation is highly dependent on the observers' experience in determining bone age.<sup>2</sup> This situation results in a serious discrepancy in the observers' evaluations. In addition, continuous time and effort are required to teach the method clinically to observers.

Deep learning, one of the advanced artificial intelligence techniques that automatically presents information derived from images, has recently gained popularity.<sup>4</sup> Based on the molar teeth in panoramic radiography, age determination can be made through artificial intelligence.<sup>5</sup> Also bone age images make an ideal database for training deep learning algorithms. Because bone X-rays exhibit a spectrum of black-white-grey tones.<sup>6</sup> Deep learning is a subclass of artificial intelligence in which artificial neural networks (ANNs) are used. The convolutional neural network (ESA) is the most frequently used ANN for image analysis and recognition. Bone age assessment is a good example of how the concept of object detection and classification can be applied. Over the last few years, significant progress has been made towards developing a digital system.<sup>7</sup> Bone age assessments have become the primary focus of the machine learning community, as the objective is typical of deep learning's object detection and classification. A corresponding side (for example, a class corresponding to a bone age) is estimated for the input of given data (for example, left hand radiography with radius of the distal bone and ulnar epiphysis). Automatic bone age assessments using ESA-based machine learning models have recently demonstrated remarkable performance.<sup>8</sup>

The purpose of this study was to transfer images to the ImageJ program using hand-wrist radiographs with varying growth development periods and to determine whether they can be used to automatically detect growth periods according to the density values obtained.

## 2 | MATERIALS AND METHODS

Ethical approval was obtained from the Clinical Research Ethics Committee of the University (09/01/2020, 2020-003).

### 2.1 | Study design

In this study, patients who were previously treated at our clinic were routinely contacted for pre-orthodontic diagnosis and treatment planning. Hand-wrist radiographs of the taken on the same day were evaluated retrospectively. The study included patients who had no known systemic disease, no growth problems, no anomalies or syndromes, and no malformations in the hand-wrist region, as well as those who had no history of trauma or pathology involving the relevant region. The study excluded patients with artefacts and distortions on hand-wrist radiographs. A total of 270 patients (135 females and 135 males) who met the necessary criteria and were between the ages of 8.3 and 17.2 enrolled in the study. All radiographs taken in our clinic are taken with the same device (Planmeca Promax, Helsinki, Finland), using the manufacturer's recommended positioning and irradiation settings.

### 2.2 | ImageJ application

The skeletal maturation stage of the individuals included in the study was determined by using the Grave and Brown<sup>9,10</sup> method. The retrospectively collected hand-wrist radiographs were classified by consensus under 7 distinct groups (PP2=, MP3=, MP3cap, DP3u, PP3u, MP3u, and Ru) that included pre-peak, peak, and post-peak stages. When determining skeletal maturation stage from hand-wrist radiographs, all radiographs were completed by two calibrated orthodontists. A third observer was consulted in case of any inconsistency. All radiographs were re-evaluated 2 weeks later by the same investigators (Ö.F.S.) and (M.H.B) to calculate intra-examiner reliability. Since the radiographs of the patients that were not suitable for analysis were not included in the measurements, the groups were not formed equally.

After converting the radiographs to TIFF format, they were imported into ImageJ 1.52a (Wayne Rasband, National Institutes of Health-NIH, Maryland, USA) (Figure 1). Hand-wrist radiographs added to ImageJ via File/Open were set with the Image/Type/32-bit command. The reason why 32-bit commands are preferred the separation in the colour spectrum over 8-bit and 16-bit commands is to provide more information and avoid losing details in the bone maturation change. The Image/Zoom/Maximize command was used to facilitate the region selection process on the analysed radiographs. It has been reported that eliminating image noise from hand-wrist radiographs is a critical step in detecting maturation.<sup>11</sup> Therefore, the Process/Noise/Despeckle command was used to create a spectrum suitable for evaluation by reducing the noise in hand-wrist radiographs (Figure 1B). The Image/Lookup Tables/Spectrum command was used to obtain the final form of the radiographs to be analysed (Figure 1C).

In all radiographs, histograms from the distal, medial, and proximal phalanx of the middle finger were obtained using the rectangle 64\*64 pixel selections tool. The region is centered on the joint space where the phalanges converge and excludes the phalanx periphery.

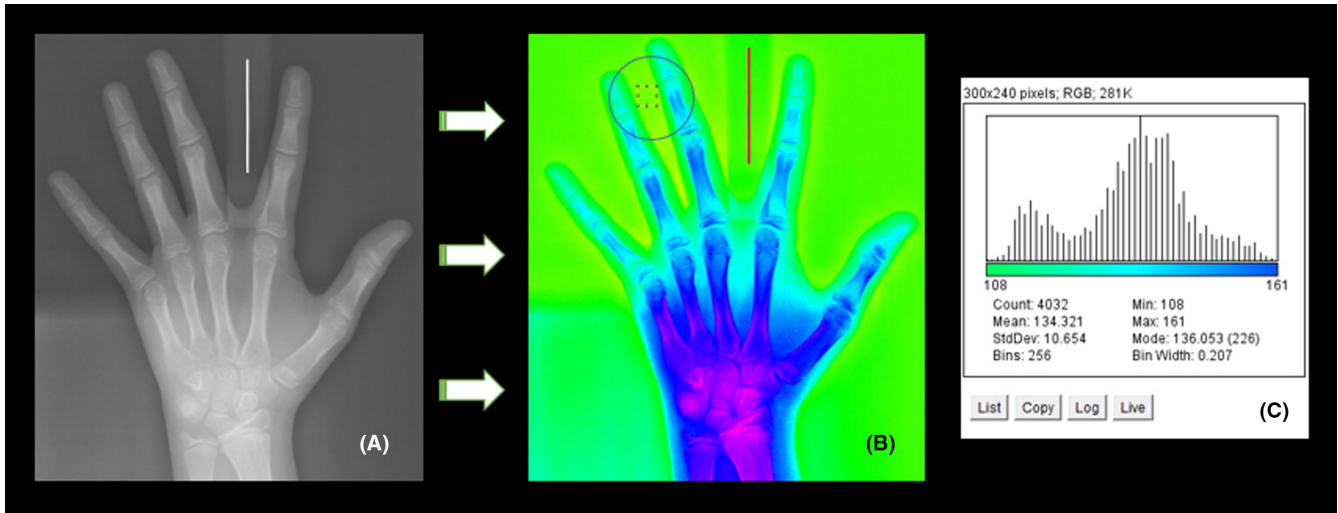


FIGURE 1 Hand-wrist radiograph of the patient (A); the pseudocolor version of the radiographs obtained in ImageJ program and the region taken as the background (B); and the Spectrum/Histogram table of the selected region on the photograph (C)

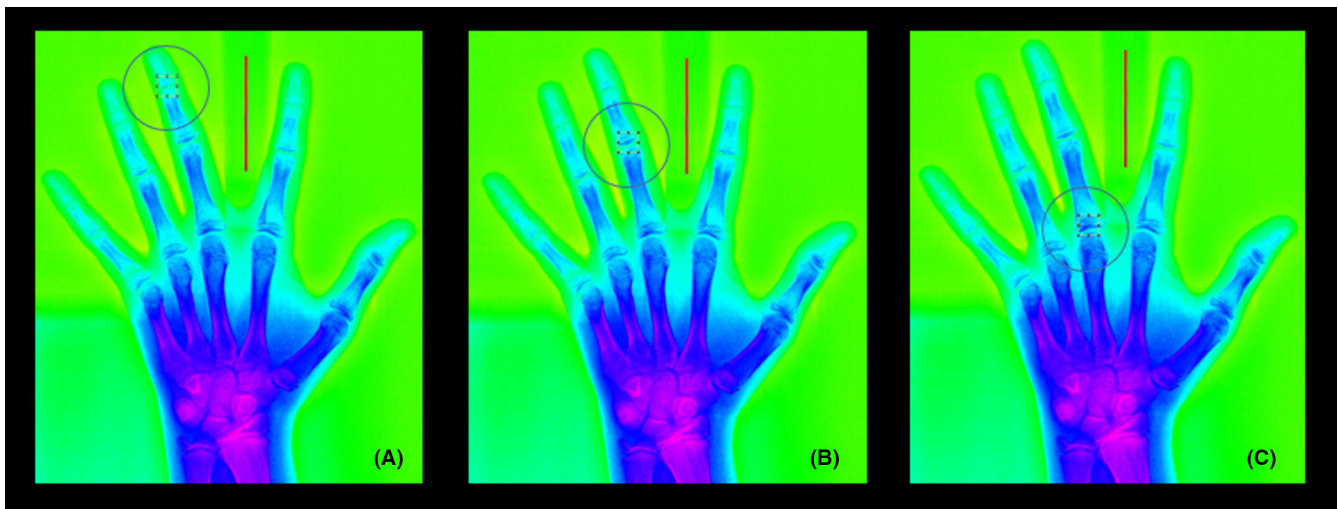


FIGURE 2 The distal (A), mesial (B), and proximal (C) phalanges of the regions examined in the pseudocolor version of the radiographs obtained in ImageJ program

In addition, in order to eliminate the density differences caused by the X-ray device in all radiographs, a histogram was created by selecting a tissue-free 64\*64-pixel area between the third and fourth fingers. The Analyse/Histogram command was used to convert the spectrum to numerical data (Figure 2). The "Mean" data obtained as a result of the analysis was used to determine the maturation stage. The distal, medial, and proximal phalanx values obtained from each radiograph were considered as their total density values (TDV). The values obtained from the tissue-free region of each radiograph were extracted from TDV by simple subtraction. The data obtained through this procedure was accepted as the pure density value (PDV). All these values were calculated for all patients, as well as by classifying them by gender.

### 2.3 | Statistical analysis

The Kolmogorov–Smirnov test was used to assess the normality of our data. Parametric tests were used because the data had a normal distribution. The Pearson chi-square test was used to determine the patients' gender distribution. The pure and total density values obtained from the medial, distal, and proximal third fingers of the hand-wrist radiographs were divided into groups of pre-peak, peak and post-peak, and, additionally, 7 different growth periods (PP2=, MP3=, MP3cap, DP3u, PP3u, MP3u, Ru) and then compared. Analysis of variance (ANOVA) was applied to evaluate the difference between the values measured by both total and gender in the groups, and pairwise comparisons were made using the post-hoc

LSD test. All radiographs were re-evaluated two weeks later by the same investigators (Ö.F.S.) and (M.H.B) to calculate intra-examiner reliability. Intra-class correlation coefficients (ICCs) were calculated to determine inter-examiner and intra-examiner reliability scores. In the inter-examiner and intra-examiner evaluations for measurement reliability, the repeatability coefficients were found to be acceptable (0.899–0.961 and 0.923–0.959, respectively). SPSS package program (for Windows, v.20.0; SPSS Inc.) was used to analyse the data. The results were considered statistically significant, being at the  $P < .05$  significance level.

### 3 | RESULTS

There was a significant difference in the ages of the groups separated according to their hand-wrist periods ( $P < .05$ ). The Pearson chi-square test revealed no statistically significant differences in the sex distribution ( $P > .05$ ) (Table 1).

There was a continuous increase in the total density values in the mesial, distal, and proximal phalanxes until the post-peak period, a decrease in density following the DP3u period until the MP3u period, and an increase in density following the MP3u period (Figure 3). There was no significant difference in the total density values of all three phalanges between the growth periods ( $P > .05$ ) (Table 1). There was a difference between the pure density values obtained after subtracting the background density from the total density values in all phalanx measurements between both male and female individuals in the groups ( $P < .05$ ). In addition, when the background densities were compared, it was determined that the groups were similar ( $P > .05$ ) (Table 1). The similarity of the backgrounds indicates that the radiograph's density and contrast are comparable, and that standardization is achieved through the comparison of the groups. In the mesial, distal, and proximal phalanxes, a continuous increase in density was observed until the post-peak period in the pure density values free from background, a decrease was observed following the DP3u period until the Ru period (Figure 4). A significant difference was observed between the growth periods in both male and female individuals in the pure density values of all three phalanges ( $P < .05$ ) (Table 1).

### 4 | DISCUSSION

When planning orthodontic treatments, it is critical to consider the individual's growth period, particularly when correcting skeletal problems. For this purpose, hand-wrist radiographs or cephalometric radiographs are taken as a diagnostic tool at the beginning of treatment in many patients. Although detection of the growth period from cervical vertebrae on cephalometric radiographs has increased in popularity in recent years, it is still considered the gold standard because hand-wrist radiographs have more specific stages for period detection, are more repeatable, and are easy to detect.<sup>12,13</sup>

Radiographic evaluation software, which is important for diagnosis in dentistry, is advancing rapidly with the advancements in modern computer technology. Artificial intelligence's applications in dentistry and orthodontics are expanding daily. There are studies and artificial intelligence software available in the literatures that examine the detection of growth period using hand-wrist radiographs and cervical vertebrae.<sup>8,14,15</sup> Our study's primary objective is to find whether the growth period can be determined from hand-wrist radiographs using the ImageJ program as an alternative to artificial intelligence software that has gained popularity in recent years.

The phases of the middle finger's distal, medial, and proximal phalanges are one of the most frequently used methods for determining the degree of maturation on hand-wrist radiographs.<sup>16</sup> In conventional radiography, the grey tones on the image correspond to the density and biological thickness of the tissues included in the image, and radiographic density differences are converted to numerical data using ImageJ and similar software, allowing for independent evaluation. Pseudocolor imaging can be obtained by using the ImageJ software's colour spectrum feature. Anatomical regions with different tissue thicknesses can be presented both visually and converted into digital data. The numerical data obtained with the ImageJ colour spectrum increases as the thickness of a tissue increase.<sup>17</sup> The increase in the thickness and density of bone tissue as the maturation phase progresses is a physiological change. According to our study's hypothesis, as the bone maturation stage progresses, the thickness of the tissue in the middle finger phalanx regions of hand-wrist radiographs and numerical data obtained using the ImageJ colour spectrum will increase.

Kök et al.<sup>15</sup> stated that while hand-wrist radiographs are the gold standard for determining maturation, cephalometrics may be preferred due to their widespread clinical use. They reported in their study that while the accuracy of maturation detection from cephalometric radiographs with the assistance of artificial intelligence was insufficient in some aspects, it was generally successful, indicating that the use of artificial intelligence in orthodontics would be beneficial.

The same researchers compared hand-wrist and cephalometric radiographs (cervical vertebrae stages) of the same individuals in another study. As a result of the study, they recommended that programs powered by artificial intelligence be used for determining maturation in order to prevent inconsistencies between observers.<sup>18</sup> In our study, we demonstrated that maturation detection using numerical data derived from standard analysis areas determined on hand-wrist radiographs independently of the observer can serve as an auxiliary and/or alternative to artificial intelligence-based software.

Kunz et al.<sup>14</sup> also investigated the use of artificial intelligence to detect landmarks in cephalometric radiography. The study mentioned the difficulty of establishing the gold standard between observers and reported that very successful results were obtained when using artificial intelligence to determine the landmark. Considering our findings, it has been determined that the maturation stage can be determined by detecting the analysis area, similar to



TABLE 1 Comparison of demographic data and density values of the groups by gender

	Sex (Female / Male)	Pre-peak period		Peak period		Post-peak period		P				
		Group I (n = 39)		Group II (n = 39)		Group III (n = 41)			Group IV (n = 37)	Group V (n = 38)	Group VI (n = 37)	Group VII (n = 39)
		PP2= Mean ± SD	MP3= Mean ± SD	MP3cap Mean ± SD	DP3u Mean ± SD	PP3u Mean ± SD	MP3u Mean ± SD					
Age	F	8.59 ± 0.42 <sup>a</sup>	11.01 ± 0.81 <sup>b</sup>	13.1 ± 0.74 <sup>c</sup>	13.88 ± 1.35 <sup>c</sup>	14.1 ± 0.54 <sup>d</sup>	14.72 ± 0.89 <sup>e</sup>	15.6 ± 1.05 <sup>f</sup>	.000			
	M	10.33 ± 0.57 <sup>a</sup>	13.14 ± 1.87 <sup>b</sup>	13.87 ± 0.99 <sup>c</sup>	14.13 ± 0.8 <sup>c</sup>	14.9 ± 0.47 <sup>d</sup>	15.48 ± 0.83 <sup>e</sup>	16.02 ± 0.86 <sup>f</sup>	.000			
	T	9.44 ± 1.51 <sup>a</sup>	12.05 ± 1.77 <sup>b</sup>	13.5 ± 1.27 <sup>c</sup>	14.01 ± 1.16 <sup>c</sup>	14.5 ± 1.28 <sup>d</sup>	15.07 ± 0.99 <sup>e</sup>	15.83 ± 0.98 <sup>f</sup>	.000			
	F/M	20 / 19	20 / 19	20 / 21	18 / 19	19 / 19	20 / 17	18 / 21	NS			
Total distal phalanx Density value	F	116.66 ± 38.13	121.01 ± 34.79	128.04 ± 29.13	129.8 ± 18.01	121.01 ± 25.66	126.1 ± 27.89	130.01 ± 28.63	NS			
	M	125.28 ± 39.55	129.36 ± 34.53	131.33 ± 23.71	144.97 ± 21.29	125.41 ± 23.08	135.08 ± 27.38	126.11 ± 27.39	NS			
	T	121.1 ± 35.52	125.08 ± 32.19	129.79 ± 26.01	136.07 ± 20.27	123.21 ± 23.73	130.23 ± 27.83	127.92 ± 31.6	NS			
Total medial phalanx Density value	F	116.91 ± 37.59	130.58 ± 34.92	138.29 ± 28.44	141.14 ± 17.38	131.55 ± 22.61	135.83 ± 26.43	139.84 ± 27.29	NS			
	M	126.28 ± 38.52	138.83 ± 34.22	141.55 ± 23.52	153.76 ± 21.44	138.45 ± 20.43	144.27 ± 27.43	135.42 ± 25.36	NS			
	T	130.34 ± 34.77	134.61 ± 31.91	140.02 ± 25.56	146.34 ± 19.58	134.98 ± 21.56	139.71 ± 26.82	137.46 ± 30.54	NS			
Total proximal phalanx Density value	F	129.23 ± 32.4	132.06 ± 33.65	150.54 ± 27.11	153.11 ± 15.35	142.04 ± 22.09	145.93 ± 26.02	150.01 ± 24.43	NS			
	M	138.2 ± 36.53	137.66 ± 34.56	152.28 ± 21.84	166.35 ± 21.64	150.42 ± 24.41	154.65 ± 30.8	145.6 ± 30.46	NS			
	T	142.07 ± 32.76	144.37 ± 31.66	151.47 ± 24.06	158.56 ± 18.79	146.23 ± 22.22	149.94 ± 27.71	147.64 ± 27.76	NS			
Background density value	F	81.37 ± 27.33	81.96 ± 33.23	89.13 ± 28.09	83.72 ± 17.17	79.56 ± 27.67	81.92 ± 28.56	86.77 ± 29.07	NS			
	M	88.64 ± 41.49	89.84 ± 35.34	85.45 ± 24.24	100.14 ± 25.79	77.37 ± 26.62	90.19 ± 23.13	83.07 ± 34.99	NS			
	T	85.1 ± 37.87	85.45 ± 32.82	87.17 ± 25.75	90.48 ± 22.02	79.01 ± 25.48	85.72 ± 26.98	84.78 ± 30.8	NS			
Pure distal phalanx Density value	F	36.95 ± 9.2 <sup>a</sup>	40.05 ± 2.31 <sup>b</sup>	38.9 ± 4.27 <sup>c</sup>	46.12 ± 5.33 <sup>d</sup>	41.43 ± 3.7 <sup>d</sup>	44.18 ± 3.83 <sup>d</sup>	43.22 ± 4.55 <sup>e</sup>	.000			
	M	36.64 ± 3.7 <sup>a</sup>	39.51 ± 4.38 <sup>b</sup>	45.88 ± 4.33 <sup>c</sup>	44.83 ± 7.44 <sup>d</sup>	46.95 ± 3.54 <sup>d</sup>	45.16 ± 5.83 <sup>d</sup>	42.23 ± 5.41 <sup>e</sup>	.000			
	T	36.71 ± 4.56 <sup>a</sup>	39.62 ± 3.99 <sup>b</sup>	42.61 ± 5.51 <sup>c</sup>	45.59 ± 6.11 <sup>d</sup>	44.19 ± 6.13 <sup>d</sup>	44.51 ± 4.5 <sup>d</sup>	43.13 ± 5.09 <sup>e</sup>	.000			
Pure medial phalanx Density value	F	44.19 ± 9.74 <sup>a</sup>	49.82 ± 2.93 <sup>b</sup>	49.16 ± 5.19 <sup>c</sup>	57.42 ± 7.04 <sup>d</sup>	51.98 ± 6.61 <sup>d</sup>	53.9 ± 4.64 <sup>e</sup>	53.06 ± 4.95 <sup>f</sup>	.000			
	M	45.54 ± 4.72 <sup>a</sup>	48.98 ± 5.32 <sup>b</sup>	56.1 ± 5.07 <sup>c</sup>	53.62 ± 7.94 <sup>d</sup>	59.94 ± 6.19 <sup>d</sup>	54.17 ± 6.72 <sup>e</sup>	52.35 ± 5.37 <sup>f</sup>	.000			
	T	45.24 ± 5.38 <sup>a</sup>	49.16 ± 4.85 <sup>b</sup>	52.85 ± 6.14 <sup>c</sup>	55.85 ± 7.43 <sup>d</sup>	55.96 ± 9.54 <sup>d</sup>	53.99 ± 5.29 <sup>e</sup>	52.68 ± 5.36 <sup>f</sup>	.000			
Pure proximal phalanx Density value	F	56.51 ± 4.92 <sup>a</sup>	60.11 ± 4.53 <sup>b</sup>	61.41 ± 5.74 <sup>c</sup>	69.39 ± 7.56 <sup>d</sup>	62.48 ± 7.79 <sup>d</sup>	64.01 ± 6.61 <sup>e</sup>	63.23 ± 7.34 <sup>f</sup>	.001			
	M	57.1 ± 6.71 <sup>a</sup>	57.81 ± 6.83 <sup>b</sup>	66.83 ± 5.88 <sup>c</sup>	66.21 ± 6.91 <sup>d</sup>	71.94 ± 2.21 <sup>d</sup>	64.63 ± 11.42 <sup>e</sup>	62.52 ± 5.47 <sup>f</sup>	.001			
	T	56.97 ± 7.85 <sup>a</sup>	58.92 ± 6.67 <sup>b</sup>	64.29 ± 6.35 <sup>c</sup>	68.08 ± 7.25 <sup>d</sup>	67.21 ± 10.99 <sup>d</sup>	64.22 ± 8.29 <sup>e</sup>	62.85 ± 7.2 <sup>f</sup>	.001			

Note: Same small superscript letter indicates no statistical difference in the column (Post-hoc LSD test).

Abbreviations: F, Female; M, Male; NS, Not-significant; P, Comparison of the density values with ANOVA test; SD, Standard Deviation; T, Total.



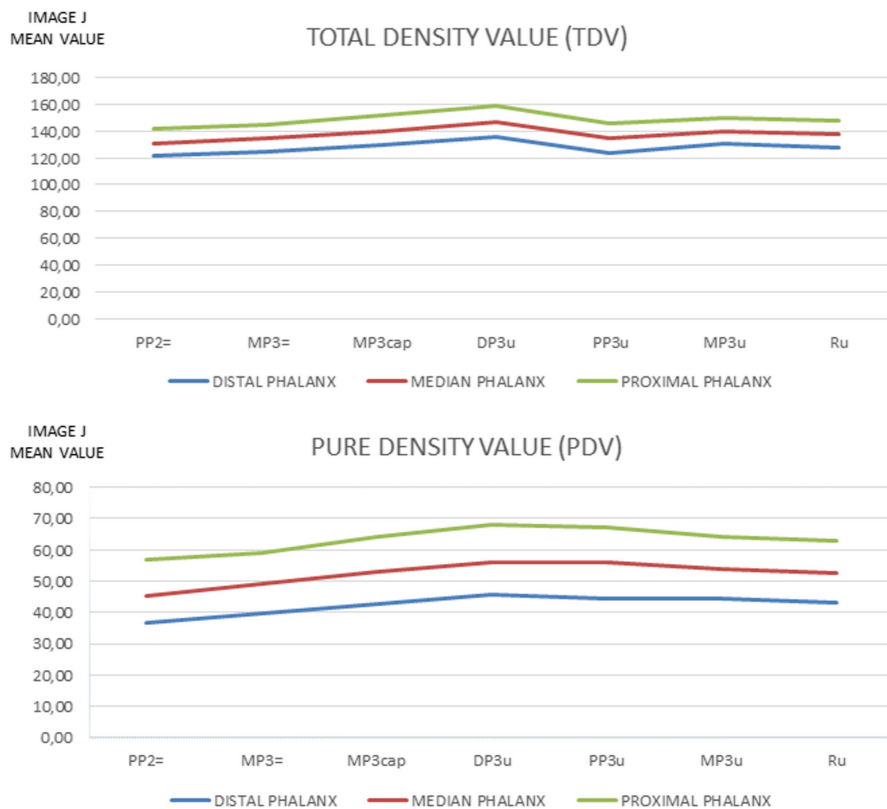


FIGURE 3 Graph of change of total density values (TDV) obtained in ImageJ program according to growth periods

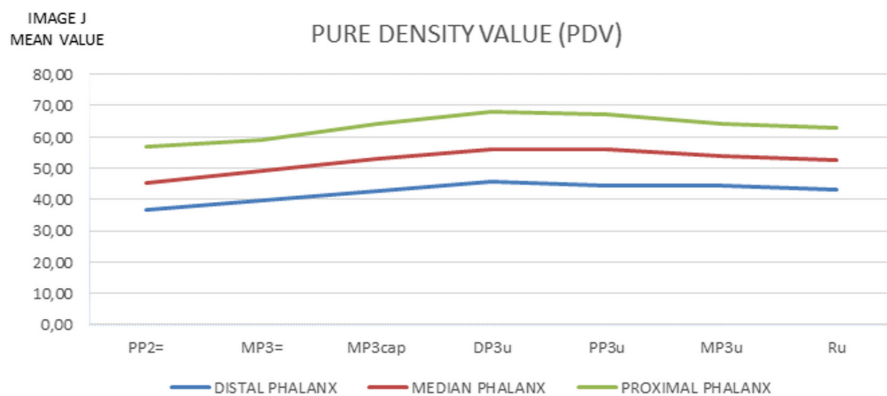


FIGURE 4 Graph of change of pure density values (PDV) obtained in ImageJ program according to growth periods

how landmarks are detected with the support of artificial intelligence from hand-wrist radiographs.

Gao et al.<sup>11</sup> detected maturation in hand-wrist radiographs using artificial intelligence supported software. They stated that the maturation detection was made more realistic by eliminating background noise in wrist radiographs. By removing the density difference in the background of hand-wrist radiographs, more acceptable results were obtained during the maturation stage in the current study. Similar to Gao et al, significant results were obtained in the PDV values obtained after removing the tissue-free region and the pre-peak period was clearly demonstrated. It should be noted that eliminating the background in numerical data in this software by a simple subtraction will not always lead to accurate results. After the pre-peak period, the PDV graph shows a slight decreasing trend in the numerical data. This result could be explained by changes in the joint space between the phalanges and in the soft tissues of the extremities following the pre-peak period.

Data is processed and classified by artificial intelligence programs. As a result, it attempts to match the shape of the area in the radiographs to be examined on a shape-based basis, and the most appropriate period is determined using artificial neural networks. The primary advantage of the ImageJ program in this case is that it enables objective evaluation of numerical data. Additionally, no prior software is required. We use the ImageJ pseudocolor application to ensure that the region of interest (ROI) for hand-wrist radiographs is accurate. Colour images provide a unique perspective and are not always used to collect numerical data.<sup>17</sup>

Further research can be conducted to obtain more detailed results by including different gender characteristics across populations

and age groups, and by conducting studies with larger sample sizes. It is even capable of establishing a norm value for each subgroup within a society. Clinicians and researchers will be able to examine individuals' the hand-wrist radiographs in ImageJ and determine their growth period based on norm values.

## 5 | CONCLUSION

In order to minimize method error in individual interpretations of hand-wrist radiographs, which enables us to determine the most reliable and specific period for detecting growth periods, many new methods such as artificial intelligence have been used recently with the advancement of technology. As a result of this preliminary study,

- It has been demonstrated that using the ImageJ program, the pure density values obtained from all phalanges of the third finger can be used to distinguish the peak growth period.
- The ImageJ program can also be used as an alternative to artificial intelligence-based growth period detection.

## AUTHOR CONTRIBUTIONS

S.S drafted the manuscript and carried out the measurements. M.H.B. and Ö.F.S. designed the study, treated the patients, and collected the data. S.S assisted in data analysis and contributed to manuscript finalization. M.H.B. drafted the manuscript and carried out the statistical analysis. S.S contributed to the analysis and revised the manuscript. T.Ç. supervised study, measurements and analysis and drafted the manuscript. All authors read and approved the final manuscript.

## CONFLICT OF INTEREST

The authors declare that there is no conflict of interests regarding the publication of this paper. (Written consent is obtained from patients who apply to our clinic for treatment purposes, indicating that their radiographs can be used scientific articles).

## DATA AVAILABILITY STATEMENT

The data that support the findings of this study are available from the corresponding author upon reasonable request.


## ETHICAL APPROVAL

The study protocol was approved by the local ethics committee (09/01/2020, 2020-003).

## CONSENT TO PARTICIPATE

Written consent is obtained from patients who apply to our clinic for treatment purposes, indicating that their radiographs or materials can be used scientific articles.

## ORCID

Muhammed Hilmi Büyükçavuş  <https://orcid.org/0000-0003-2184-1549>

## REFERENCES

- Tang FH, Chan JLC, Chan BKL. Accurate age determination for adolescents using magnetic resonance imaging of the hand and wrist with an artificial neural network-based approach. *J Digit Imaging*. 2019;32(2):283-289.
- Creo AL, Schwenk WF 2nd. Bone age: a Handy tool for pediatric providers. *Pediatrics*. 2017;140(6):e20171486.
- De Sanctis V, Di Maio S, Soliman AT, Raiola G, Elalaily R, Millimaggi G. Hand X-ray in pediatric endocrinology: skeletal age assessment and beyond. *Indian J Endocrinol Metab*. 2014;18(Suppl 1):S63-S71.
- Cheng CT, Ho TY, Lee TY, et al. Application of a deep learning algorithm for detection and visualization of hip fractures on plain pelvic radiographs. *Eur Radiol*. 2019;29(10):5469-5477.
- Kim S, Lee YH, Noh YK, Park FC, Auh QS. Age-group determination of living individuals using first molar images based on artificial intelligence. *Sci Rep*. 2021;11(1):1073.
- Wang F, Gu X, Chen S, et al. Artificial intelligence system can achieve comparable results to experts for bone age assessment of Chinese children with abnormal growth and development. *PeerJ*. 2020;8:e8854.
- Spampinato C, Palazzo S, Giordano D, Aldinucci M, Leonardi R. Deep learning for automated skeletal bone age assessment in X-ray images. *Med Image Anal*. 2017;36:41-51.
- Lee BD, Lee MS. Automated bone age assessment using artificial intelligence: the future of bone age assessment. *Korean J Radiol*. 2021;22(5):792-800.
- Grave KC, Brown T. Skeletal ossification and the adolescent growth spurt. *Am J Orthod*. 1976;69(6):611-619.
- Iguma KE, Tavano O, Carvalho IM. Comparative analysis of pubertal growth spurt predictors: martins and Sakima method and Grave and Brown method. *J Appl Oral Sci*. 2005;13(1):58-61.
- Gao Y, Zhu T, Xu X. Bone age assessment based on deep convolution neural network incorporated with segmentation. *Int J Comput Assist Radiol Surg*. 2020;15(12):1951-1962.
- Proffit WR, Fields HW, Sarver DM. *Contemporary Orthodontics*. Mosby Elsevier; 2007.
- Prokop-Piotrkowska M, Marszałek-Dziuba K, Moszczyńska E, Szalecki M, Jurkiewicz E. Traditional and new methods of bone age assessment-an overview. *J Clin Res Pediatr Endocrinol*. 2021;13(3):251-262.
- Kunz F, Stellzig-Eisenhauer A, Zeman F, Boldt J. Artificial intelligence in orthodontics: evaluation of a fully automated cephalometric analysis using a customized convolutional neural network. *J Orofac Orthop*. 2020;81(1):52-68.
- Kök H, İzgi MS, Acilar AM. Determination of growth and development periods in orthodontics with artificial neural network. *Orthod Craniofac Res*. 2021;24(Suppl 2):76-83.
- Fishman LS. Radiographic evaluation of skeletal maturation. A clinically oriented method based on hand-wrist films. *Angle Orthod*. 1982;52(2):88-112.
- Satir S, Büyükçavuş MH, Orhan K. A novel approach to radiographic detection of bucco-palatal/lingual dilacerations: a preliminary study with ImageJ. *Proc Inst Mech Eng H*. 2021;235(11):1310-1314.
- Kök H, Acilar AM, İzgi MS. Usage and comparison of artificial intelligence algorithms for determination of growth and development by cervical vertebrae stages in orthodontics. *Prog Orthod*. 2019;20(1):41.

**How to cite this article:** Şatir S, Büyükçavuş MH, Sari ÖF, Çimen T. A novel approach to radiographic detection of growth development period with hand-wrist radiographs: A preliminary study with ImageJ imaging software. *Orthod Craniofac Res*. 2022;00:1-7. doi: [10.1111/ocr.12584](https://doi.org/10.1111/ocr.12584)